

Georadar processing and imaging with Gabor deconvolution - Houston Coastal Center

Adrian D. Smith, Robert J. Ferguson, and Robert R. Stewart

ABSTRACT

A 2D line from a georadar (GPR) dataset was collected at the Houston Coastal Center in 2012, aiming to image a series of culverts underneath a road bridge. We processed the line using a Gabor deconvolution workflow instead of traditional processing methods. We find that Gabor deconvolution is able to correct for attenuation and greatly improve resolution and signal bandwidth at late arrival times. Diffraction imaging velocities were estimated by hyperbola fitting and the dataset was imaged using zero-offset Gazdag migration to collapse the hyperbolic events on the section. We also used shot-record Gazdag Prestack Depth Migration (PSDM) to give an improved image. As we are dealing with circular reflector geometry and not point diffractors, we apply a correction factor to the diffraction velocity to obtain a more accurate image after migration. Certain features are visible in the deconvolved section, possibly including the steeply dipping flanks of the edge of the bridge. In the future we hope to refine our velocity model to take into account lateral velocity variations, and process and image the other three surveys in the dataset.

INTRODUCTION

The Houston Coastal Center georadar (GPR) dataset was acquired over a number of targets near the Houston Coastal Center, located near La Marque Texas, United States. Four surveys were acquired, including a 3D grid in 2010 and three 2D lines in 2012 (Figure 1, Table 1). There is a series of four metal culverts running through a bridge under the roadway on the western edge of the area (Figure 1). These culverts prove an interesting imaging target and are likely the reason for the original 3D grid survey that was acquired in 2010. The four surveys were acquired using a bistatic time-domain georadar system with a transmitter-receiver antenna separation of 0.28 m.

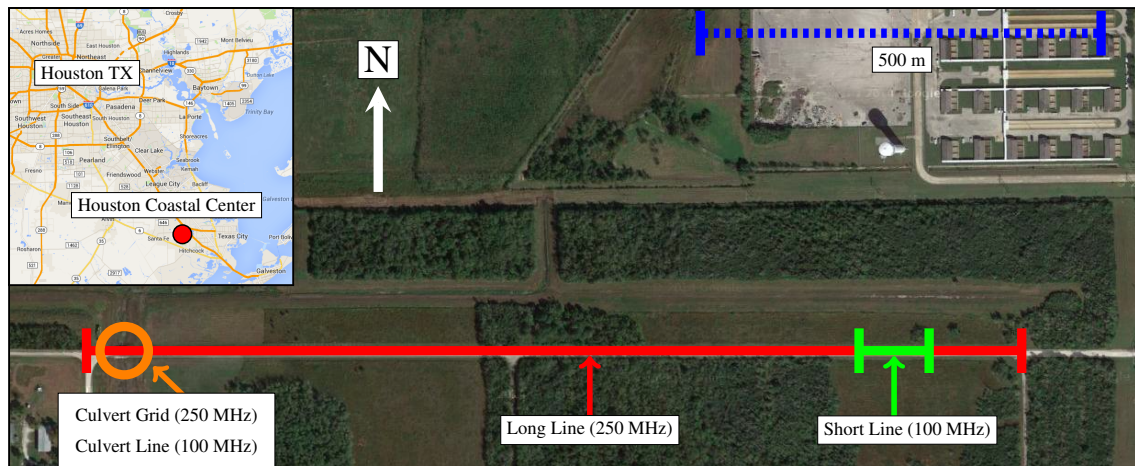


FIG. 1. Site map of the Houston Coastal Center. The approximate location of the four georadar surveys on-site is highlighted. The parameters for each individual survey are shown in Table 1. *satellite imagery courtesy of Google Maps 2014.*

	Culvert Grid	Culvert Line	Long Line	Short Line
Filename	Grid 5	Project 7, Line 01	Project 0, Line 0	Project 7, Line 00
Date	3/18/2010	3/4/2012	3/4/2012	3/4/2012
Antenna Frequency	250 MHz	100 MHz	250 MHz	100 MHz
Survey Dimensions	22m x 4m (0.5m line spacing)	25 m	1050 m	100 m
Step Size (m)	0.05	0.1	0.05	0.1
Stacks	32	128	4	128
Sample Rate (ns)	0.4	0.8	0.4	0.8
GPS	Yes	No	Yes	No

Table 1. Parameters of the four georadar surveys acquired at the Houston Coastal Center, with locations shown in Figure 1.

Figure 2 illustrates the geometry of the 3D grid along with the approximate location of the more recent Culvert Line survey (Project 7, Line 01) relative to the grid. Figure 3 shows a cross-sectional view of the culverts. The depth from the road surface to the top of each of the culverts is about 0.75 m, and the depth to the top of the water/grass at the base of the culverts being just over 3 m. As well, there are soil/concrete transitions near the bridge both at a constant depth everywhere of about 0.4 m which is the base of the roadway, and relatively steeply dipping at either side of the bridge. These interfaces are all potentially resolvable using georadar.



FIG. 2. Georadar survey geometry over the culverts at the Houston Coastal Center. In the Culvert Grid survey, there are a total of 7 lines running in an East-West direction and 44 running in a North-South direction. The Culvert Line survey (Project 7, Line 01) is approximately co-located with grid line X6. Table 1 contains parameters for both surveys. *satellite imagery courtesy of Google Maps 2014.*

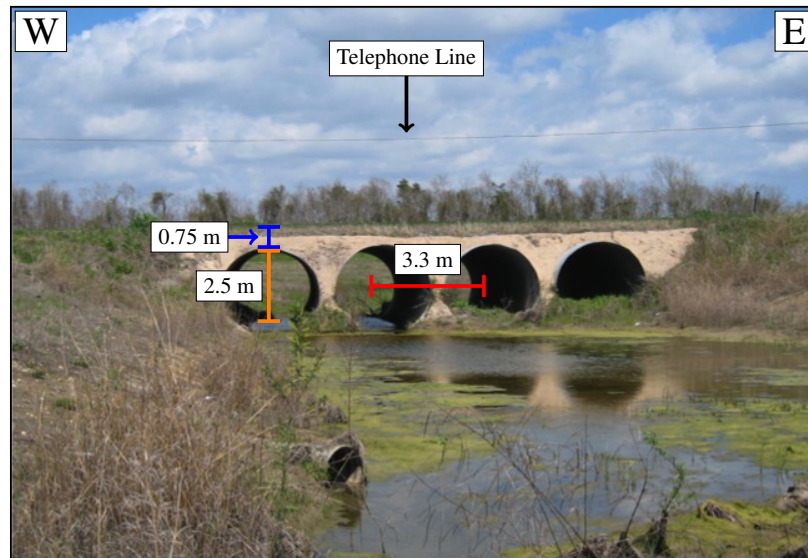


FIG. 3. Cross-sectional view of the culverts at the Houston Coastal Center. The distance from the road surface ($z = 0$ m) to the top of the culverts, the distance from the top of a culvert to its base, and the separation of the centers of two adjacent culverts are shown. All distances are approximate. Also note the location of a telephone line over the survey area.

We describe our work the 2D Culvert Line exclusively in this report. Eventually, we would like to process and image all four of the surveys in the dataset.

PROCESSING WORKFLOW

It has been shown in previous work that seismic-based processing flows are superior to more traditional georadar processing flows (Ferguson et al., 2012). The major difference between them is the absence of a *de-wow* filter and the application of Gabor nonstationary deconvolution (as summarized in Margrave et al. (2011)) in the seismic-based processing flow. We believe that Gabor deconvolution provides better results due to its ability to account for Q attenuation, which is about an order of magnitude smaller (resulting in a larger attenuation effect) than with seismic data (Ferguson and Margrave, 2012). Our processing flow is summarized in Table 2.

Process	Parameters
(1) Time Zero	8 ns shift
(2) Top Mute	0 – 13 ns
(3) Gabor Deconvolution	<p>(<i>gabordecon</i> from the CREWES processing toolbox)</p> <p>$twin = 10/f_{Nyq}$, $tinc = 1/2f_{Nyq}$, $tsmo = 50/f_{Nyq}$, $fsmo = 87$ MHz, Hyperbolic smoothing, $stab = 0$, Minimum phase, Synthesis window is unity, $gbd = 60$</p>
(4) Bandpass Filter	$0.05f_{Nyq} - 0.6f_{Nyq}$ (31 – 375 MHz)

Table 2. Seismic-based Gabor deconvolution processing parameters based on the workflow developed in Ferguson et al. (2012). f_{Nyq} is the Nyquist frequency of the data, which is 625 MHz for the Culvert Line.

The raw georadar record for the Culvert Line survey is displayed in Figure 4a. Notice that zero time does not occur at the beginning of the record, with data at negative recording time. We applied a time shift of 8 ns to eliminate the negative time region, resulting in the image in Figure 4b.

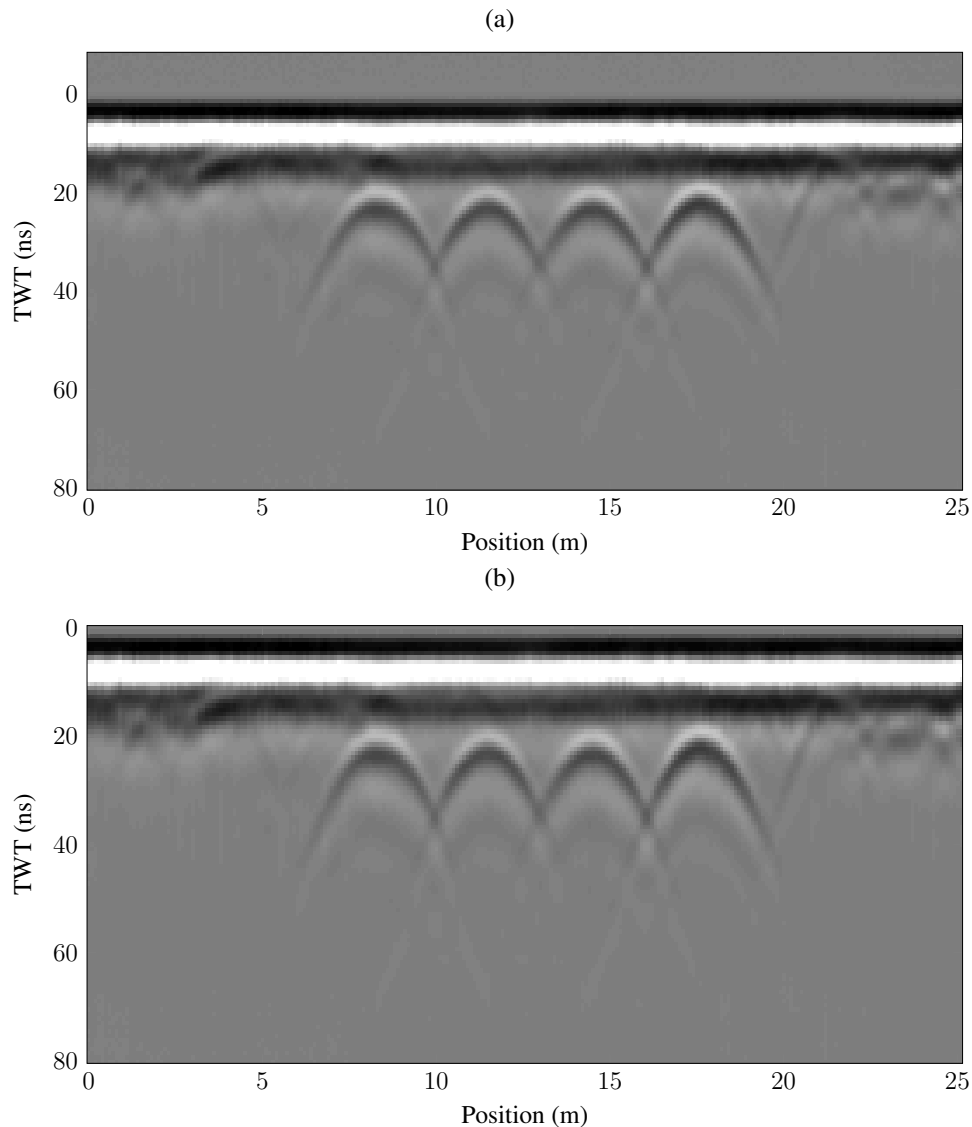


FIG. 4. (a) Culvert Line raw georadar record. (b) Raw data shifted to zero time.

Before Gabor deconvolution, we apply an early time mute to suppress the high amplitude airwave from the signal. We then perform Gabor deconvolution on both the unmuted (Figure 5a) and muted (Figure 5b) records to compare the effect of the mute. There were some issues with the *gabordecon* code working properly for certain parameters, but we tried to follow these rules of thumb for Gabor deconvolution from Ferguson et al. (2012) and Margrave et al. (2011) as best we could:

- Use hyperbolic smoothing
- The frequency smoother (*fsmo* in *gabordecon*) should be close to the centre frequency (f_c) of the data
- The Gaussian width (*twin*) should be about the width of the wavelet

- The temporal smoother (tsmo) should be about 5 times the Gaussian width

The centre frequency (f_c) of the data was calculated by finding the frequency corresponding to the maximum value of the amplitude spectrum of a brute trace stack. We calculated it to be about 87 MHz, which is very close to the antenna frequency (100 MHz) for the Culvert Line (Table 1). We used this f_c value of 87 MHz as the frequency smoother in our deconvolutions (Table 2).

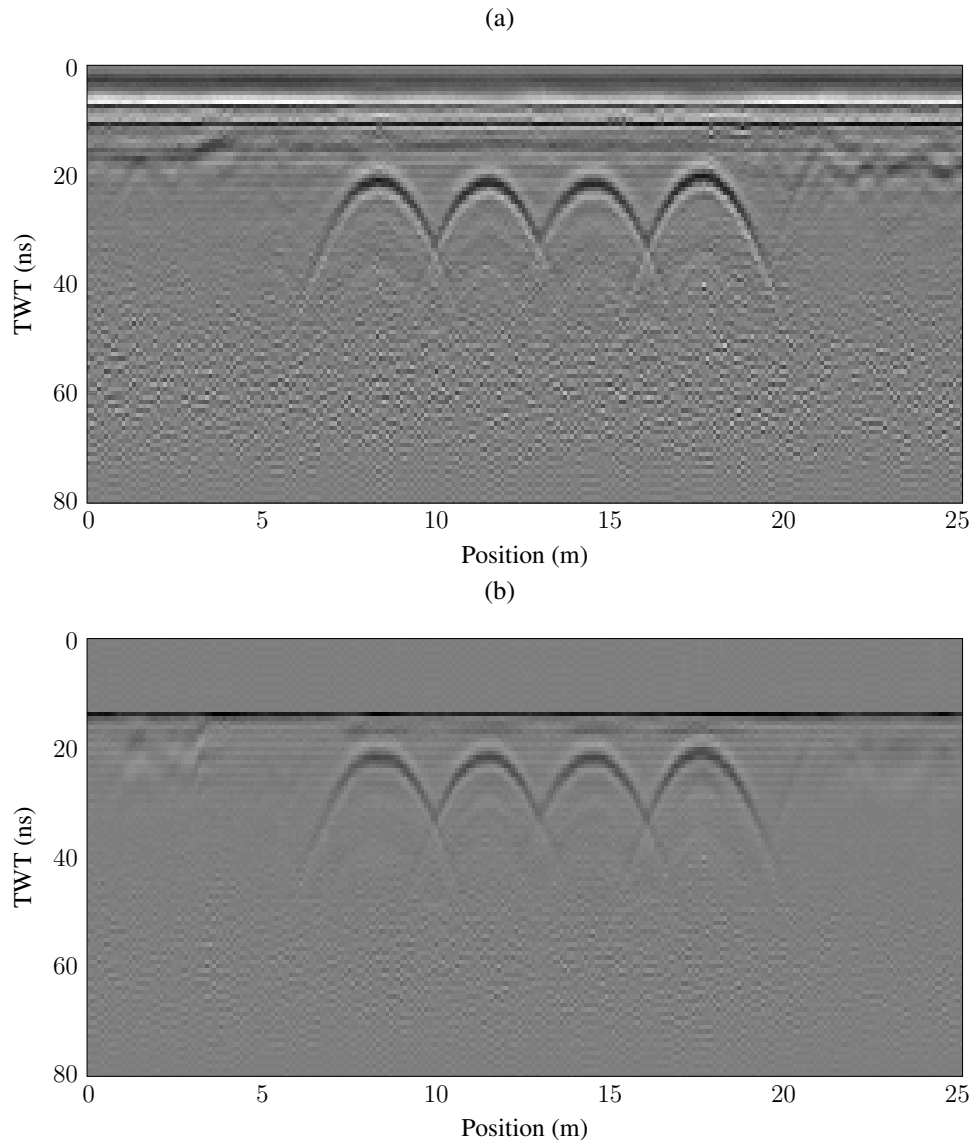


FIG. 5. Culvert Line after Gabor deconvolution. (a) No mute applied, (b) mute applied from 0 – 13 ns prior to deconvolution.

We applied a bandpass filter in order to remove noise artificially amplified by deconvolution. Our filter parameters of $0.05f_{Nyq} - 0.6f_{Nyq}$ (31 – 375 MHz) were chosen in order to eliminate high-frequency ringing visible at about the 20 ns mark in both the unmuted

(Figure 5a) and muted (Figure 5b) sections as well as any remaining DC bias in the signal. The post-deconvolution filtered sections (both unmuted and muted) are shown in Figure 6.

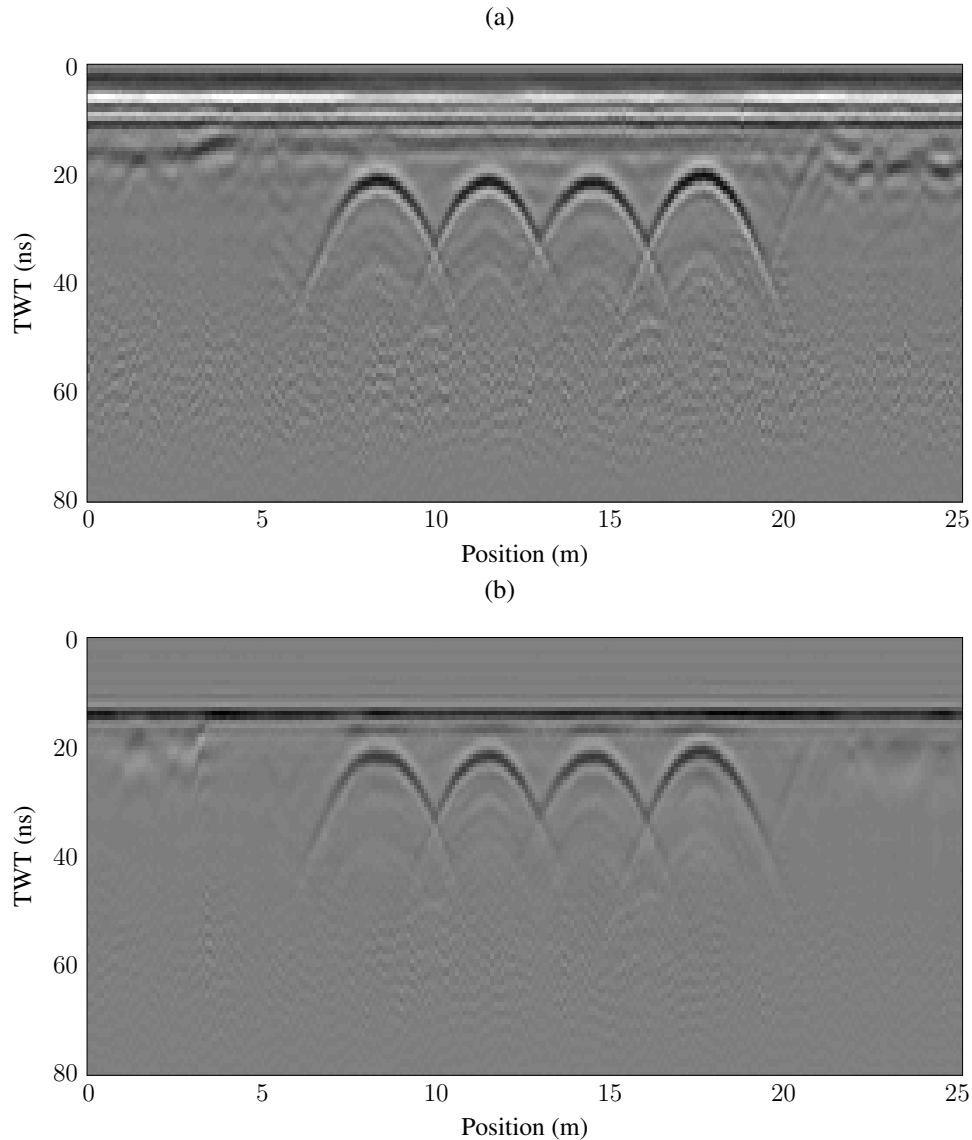


FIG. 6. Gabor deconvolved Culvert Line after bandpass filtering. (a) No mute applied, (b) mute applied from (0 – 13) ns prior to deconvolution.

Observations

The Gabor deconvolution workflow greatly improves the signal quality at later times relative to the raw record without the need to apply either a *dewow* filter or a form of automatic gain control (AGC). We can see useful reflection energy down to about 40 – 50 ns, and deconvolution improves the resolution of both the hyperbolic signatures from the top of the culverts as well as the reflection energy located at about 20 ns on either side of the bridge.

The top mute is not particularly effective at removing the airwave signature in a manner that improves the deconvolution result. As the thin near-surface layers such as the roadway are within close proximity of the airwave in time, we have removed them when applying the top mute. Also, it causes amplitude scaling issues in the output because the first non-zero samples are still much higher amplitude than the rest. This causes the appearance of a strong amplitude linear reflector at 14 ns (Figure 5b) which is not visible on the unmuted deconvolved section (Figure 5a).

The application of the bandpass filter successfully removed the high-frequency noise visible in Figure 5a from about 15 to 30 ns without significantly reducing the reflectivity from the features at about 20 ns from 0-4 and 21-25 m. We also notice a steeply dipping event in Figure 6a at about 20 m with contrasting signal character on either side of it. This may represent the lateral edge of the bridge as observed in Figure 3. On the opposite side, we see a similar change in signal character at about 5 m, although any sign of a reflection is much weaker. This may be because the boundary appears steeper on this side looking at the picture of the bridge (Figure 3). We use the unmuted filtered section after Gabor deconvolution displayed in Figure 6a as our input dataset for imaging.

VELOCITY ANALYSIS AND IMAGING

We perform preliminary depth migrations of the processed georadar record from the Culvert Line. First, we fit hyperbolae to the culvert reflection signatures to obtain velocities that will collapse them to diffraction points under migration. We generate a constant velocity model using these diffractor velocities and depth image using both zero-offset Gazdag migration and shot-record Gazdag Prestack Depth Migration (PSDM). We then apply a correction to the velocity model to account for the circular geometry of the culverts and re-image.

Hyperbola fitting

We obtain velocity information from fitting diffraction hyperbolae to the processed section as we have no multi-offset data. We fitted hyperbolae to each of the culvert reflection signatures (Figure 7). The geometric properties of each of the four hyperbolae are in Table 3.

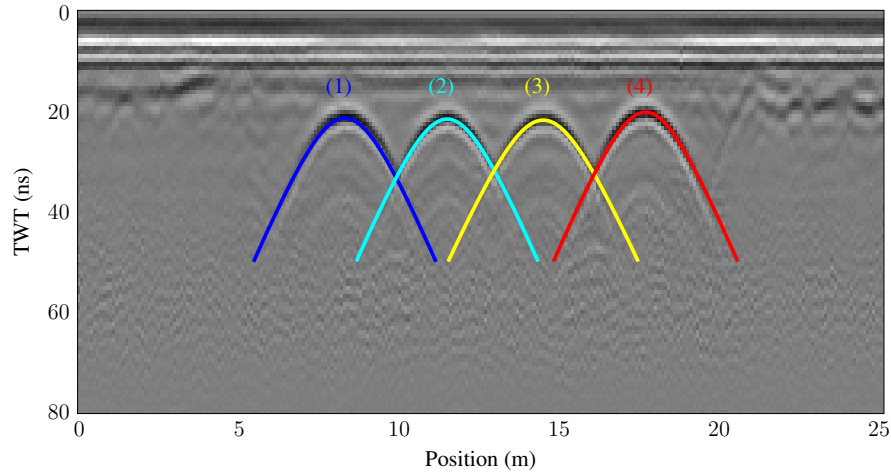


FIG. 7. Input section for imaging (Figure 6a) with best-fitting diffraction hyperbolae placed over all of the reflection signatures culvert reflections. Parameters of all four hyperbolae are given in Table 3

Hyperbola	1	2	3	4
t_0 (ns)	21.2	21.4	21.6	20.0
x_0 (m)	8.3	11.5	14.5	17.7
v_D ($\%c$)	0.42	0.42	0.44	0.42

Table 3. Best fitting parameters for the four hyperbolic reflection signatures in Figure 7. t_0 is the two-way travelttime (TWT) to the apex of each diffraction hyperbola, x_0 is the horizontal position of each apex, and v_D is the velocity that gives the best fitting hyperbola. c is the speed of electromagnetic radiation in a vacuum.

Zero-offset Gazdag migration

Using the velocities obtained from hyperbola fitting, we perform zero-offset Gazdag migration (Gazdag, 1978) to depth image the processed record in Figure 6a. We use a constant velocity model. Parameters used in the migrations are given in Table 4. Our velocity model only extends to a depth of 3 m as this represents a reasonable maximum depth of investigation. Figure 8a shows the resulting depth-migrated section using the average of the four diffractor velocities, which is $0.425c$ where c is the speed of electromagnetic radiation in a vacuum.

Parameter	f_{min}	f_{max}	dz	z_{max}	dx
	1 MHz	313 MHz	0.01 m	3 m	0.1 m

Table 4. Migration parameters.

We observe that the diffraction hyperbola-fitted velocities successfully collapse the energy onto points (Figure 8a). However, we note that this is not a true representation of the subsurface structure as we would expect to observe circular, culvert structures. This is due to an ambiguity in reflector geometry and velocity on zero/common-offset data that is addressed in Smith and Ferguson (2014). We assume that the culverts take on a roughly circular shape, with an approximate radius of 1.5 m (Figure 3). Using the relationship between diffractor (v_D) and circular (v_C) velocity outlined in Smith and Ferguson (2014), we find that the RMS velocity of the medium above the culverts is related to the diffractor velocity by the following relation:

$$v_C(r, v_D)|_{r=1.5} = 0.864v_D. \quad (1)$$

As v_D is about $0.425c$ in this case as determined from diffraction hyperbola fitting, we calculate v_C to be about $0.368c$. We generate another constant velocity model with this geometrically-corrected value and migrate using zero-offset Gazdag migration, with the result in Figure 8b.

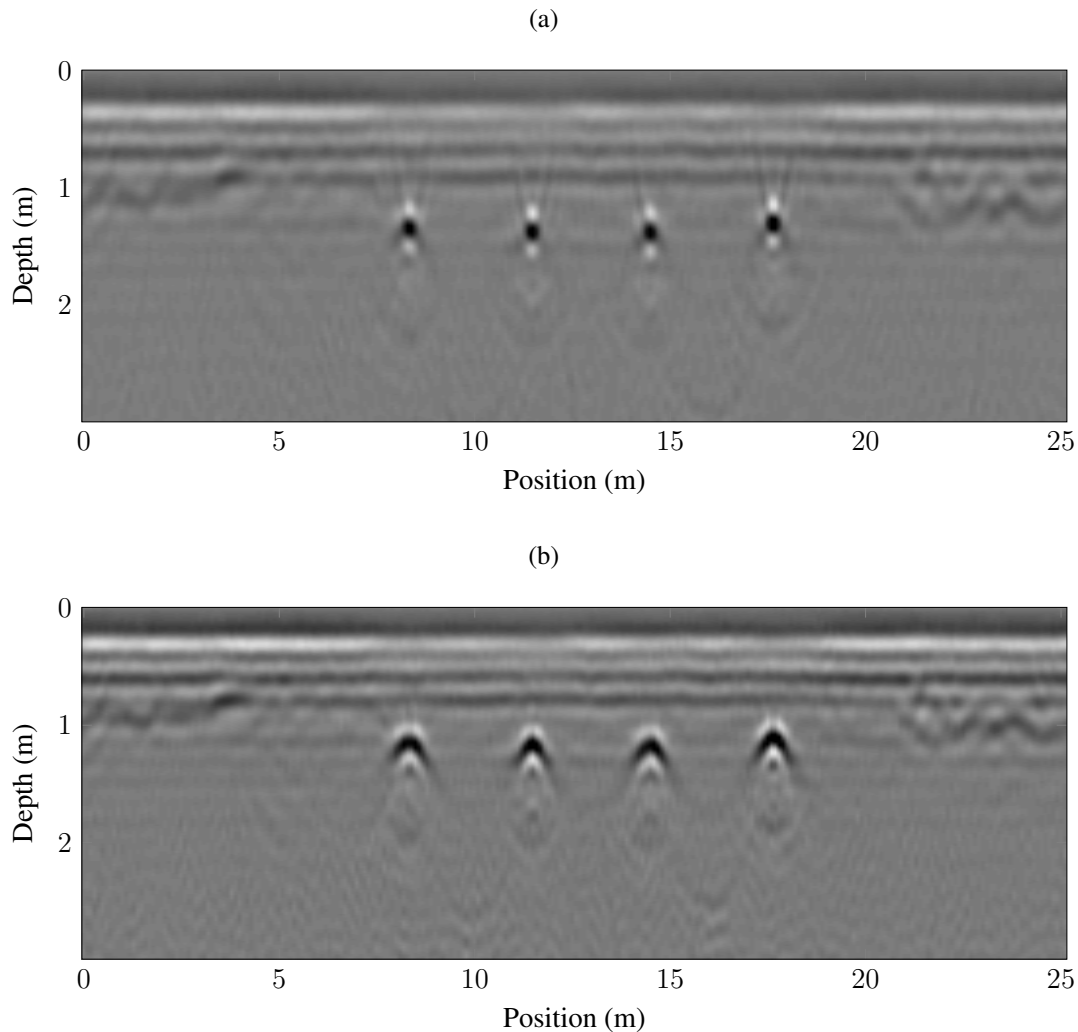


FIG. 8. Zero-offset Gazdag migrated sections. (a) Constant velocity medium of $0.425c$, determined from diffraction hyperbola fitting. (b) Velocity model corrected for circular geometry, constant velocity of $0.368c$. Both images are 3x vertically exaggerated.

Shot-record Gazdag PSDM

We performed shot-record Gazdag PSDM (Gazdag, 1978) using the same two constant velocity models as in the zero-offset case. The input georadar section is not truly zero-offset as there is a small offset between transmitter and receiver antennae, so PSDM should account for this and generate a better, more focused image. We treat each trace in the input georadar record as being the only non-zero trace in a symmetric shot record with a slight offset from the source location positioned at the centre of the record. We migrate trace by trace and stack the results together to obtain the final image. We use the same migration parameters as in the are given in Table 4.

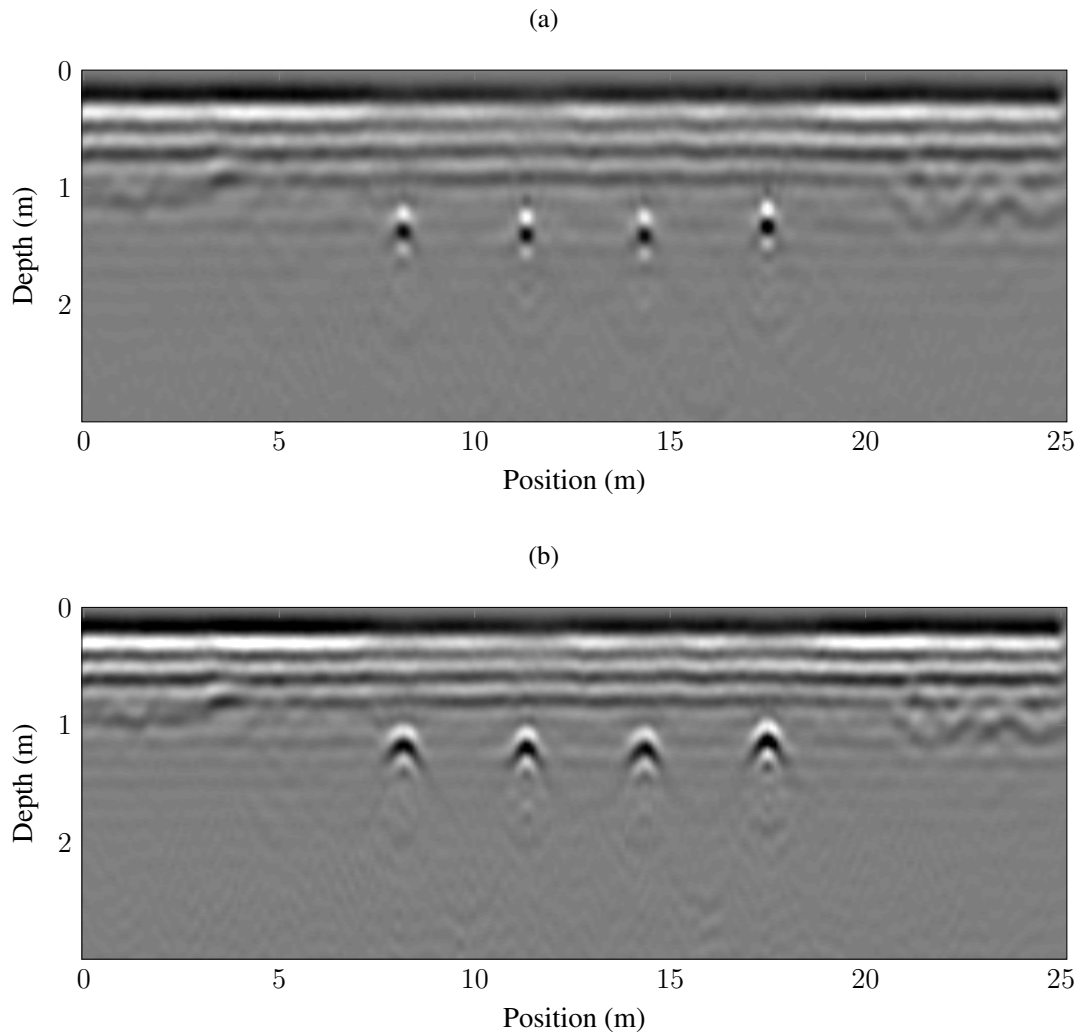


FIG. 9. Shot-record Gazadag PSDM sections. (a) Constant velocity medium of $0.425c$, determined from diffraction hyperbola fitting. (b) Velocity model corrected for circular geometry, constant velocity of $0.368c$. Both images are 3x vertically exaggerated.

Migration comparison

When we compare the results between our zero-offset migrations in Figure 8 and our shot-record migrations in Figure 9, we observe noticeable improvement. Comparing the migrations using the diffractor velocity model (Figures 8a and 9a), we notice that the energy is collapsed to the diffraction points much better in the PSDM record, as we can see "smiles" observed above the top of the arches at approximately 1 m depth on the zero-offset migrated section. We also note that in both the zero-offset and shot-record migrated sections, the image using the velocity-corrected image appears clearer and more focused, especially at shallow depths. The change in reflection character at about 1 m depth and 20 m horizontal position is also better focused. This could be interpreted as the change from concrete comprising the bridge to soil.

Figure 10 contains portions of the images of migrations performed with the circular correction applied to the diffractor velocity, displayed at a 1-1 scale. We notice that there is less scattered energy around the culvert located at about 17.5 m position. Also, the events up shallow in the section are much better focused in the shot-record migrated section than in the zero-offset migrated one. However, we notice that the culvert in the image does not appear as curved as the actual culvert (Figure 3). We surmise that although the geometry-corrected velocity is better than the diffractor velocity, it is still higher than the true medium velocity. This is possibly because the velocity correction in Smith and Ferguson (2014) was derived for true zero-offset acquisition geometry, whereas this is bistatic data. Our choice of r may also be incorrect.

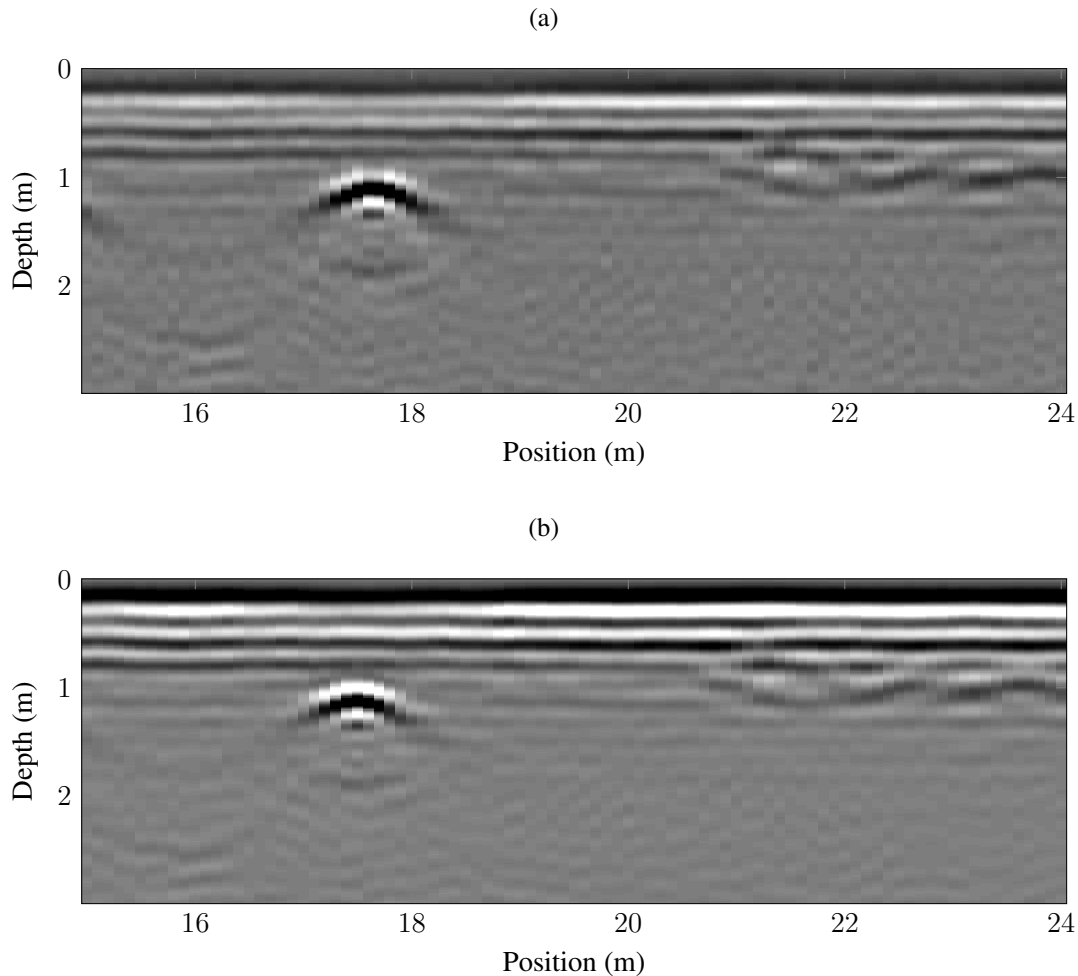


FIG. 10. Portion of zero-offset Gazdag migrated (10a) and shot-record Gazdag PSDM (10b) sections from the full migrated images in Figures 8 and 9. Displayed at a 1-1 scale.

CONCLUSIONS

We processed and performed preliminary depth imaging on a 2D georadar line from a dataset acquired at the Houston Coastal Center. This survey was of particular interest as it targeted a number of circular culverts. We used a Gabor deconvolution workflow

to preprocess the data for imaging. We found that the best results were obtained when no mute was applied prior to deconvolution and a bandpass filter applied after. Although limited slightly by technical difficulties with the *gabordecon* code, we need to do further work to optimize the Gabor deconvolution parameters.

We used hyperbolic fitting of the culvert reflection signature to estimate velocities that would collapse the signatures to points, which we did with zero-offset Gazdag migration. We then applied a circular geometrical correction factor to the constant-velocity model for migration, giving a better depth image of the culverts. We migrated both velocity models with shot-record Gazdag PSDM, giving noticeably better results especially up shallow in the section.

Future work

The Houston Coastal Center georadar dataset provides an excellent source to test processing and imaging workflows as it provides data with different frequency characteristics and interesting imaging targets. There are three other surveys (two lines and a 3D grid) not discussed here that can be used in the future to test both the Gabor nonstationary deconvolution workflow as well as various velocity model building and imaging techniques. Of particular interest is the 3D grid. An ultimate goal would be to develop a laterally varying velocity model and 3D image of the bridge region. To do so would require a different imaging algorithm, one possibility being Phase-Shift Plus Interpolation (PSPI). These velocity-model building techniques could be applied to other georadar datasets with similar targets. Finally, this dataset presents a test case to test developments with applying corrections to diffractor velocities in situations with non-diffractor geometries.

ACKNOWLEDGEMENTS

We thank the sponsors of CREWES for their support. We also gratefully acknowledge support from NSERC (Natural Science and Engineering Research Council of Canada) through the grant CRDPJ 379744-08. We would also like to thank the University of Houston for providing the Houston Coastal Center georadar dataset.

REFERENCES

- Ferguson, R. J., Ercoli, M., and Frigeri, A., 2012, Georadar data processing and imaging: paleoseismicity in the piano di castelluccio basin, central italy: CREWES Research Report, **24**.
- Ferguson, R. J., and Margrave, G. F., 2012, Attenuation compensation for georadar data by gabor deconvolution: CREWES Research Report, **24**.
- Gazdag, J., 1978, Wave equation migration with the phase-shift method: *Geophysics*, **43**, No. 7, 1342–1351.
- Margrave, G. F., Lamoureux, M. P., and Henley, D. C., 2011, Gabor deconvolution: Estimating reflectivity by nonstationary deconvolution of seismic data: *Geophysics*, **76**, No. 3, W15–W30.
- Smith, A. D., and Ferguson, R. J., 2014, Geometrical corrections for poststack imaging focusing velocity analysis: CREWES Research Report, **26**.